CAM 89-32

SIAM J. NUMER. ANAL.
Vol. 28, No. 4, pp. 907–922, August 1991

002

HIGH-ORDER ESSENTIALLY NONOSCILLATORY SCHEMES FOR HAMILTON–JACOBI EQUATIONS*

STANLEY OSHER† AND CHI-WANG SHU‡

Abstract. Hamilton–Jacobi (H-J) equations are frequently encountered in applications, e.g., in control theory and differential games. H-J equations are closely related to hyperbolic conservation laws—in one space dimension the former is simply the integrated version of the latter. Similarity also exists for the multidimensional case, and this is helpful in the design of difference approximations. In this paper high-order essentially nonoscillatory (ENO) schemes for H-J equations are investigated, which yield uniform high-order accuracy in smooth regions and sharply resolve discontinuities in the derivatives. The ENO scheme construction procedure is adapted from that for hyperbolic conservation laws. The schemes are numerically tested on a variety of one-dimensional and two-dimensional problems, including a problem related to control optimization, and high-order accuracy in smooth regions, good resolution of discontinuities in the derivatives, and convergence to viscosity solutions are observed.

Key words. essentially nonoscillatory schemes, Hamilton–Jacobi equations

AMS(MOS) subject classifications. 35L99, 65M05

1. Introduction.

The Hamilton-Jacobi (H-J) equation

$$\phi_t + H(\phi_{x_1}, \cdots, \phi_{x_d}) = 0, \qquad \phi(x, 0) = \phi_0(x) \tag{1.1}$$

appears often in applications, e.g., in control theory and differential games. The solutions to (1.1) typically are continuous but with discontinuous derivatives, even if the initial condition $\phi_0(x)$ is C^∞. The nonuniqueness of such solutions to (1.1) also necessitates the introduction of the notions of entropy conditions and viscosity solutions, to single out a unique practically relevant solution. See, e.g., Crandall and Lions [1] for details.

An important class of numerical methods for solving (1.1) is the class of monotone schemes discussed by Crandall and Lions [2]. Monotone schemes are proven convergent to the viscosity solutions. Unfortunately monotone schemes are at most first-order accurate. Traditional high-order methods are unsuitable, because spurious oscillations will generally occur in the presence of discontinuous derivatives.

There is a close relation between (1.1) and a hyperbolic conservation law

$$u_t + \sum_{i=1}^{d} f_i(u)_{x_i} = 0, \qquad u(x, 0) = u_0(x). \tag{1.2}$$

In fact, for the one-dimensional case $d = 1$, (1.1) is equivalent to (1.2) if we take $u = \phi_x$. For multidimensions this direct correspondence disappears, but in some sense we can still think about (1.1) as (1.2) "integrated once." Hence successful numerical methodology for solving hyperbolic conservation laws (1.2) should also be applicable to the H-J equation (1.1).

* Received by the editors December 26, 1989; accepted for publication (in revised form) October 9, 1990.

† Department of Mathematics, University of California, Los Angeles, California 90024. This research was supported by National Science Foundation grant DMS 88-11863, Defense Advanced Research Projects Agency grant in the Applied and Computational Mathematics Program, Office of Naval Research grant N00014-86-K-0691, and National Aeronautics and Space Administration Langley grant NAG-1-270.

‡ Division of Applied Mathematics, Brown University, Providence, Rhode Island 02912. This research was supported by National Science Foundation grant DMS 88-10150 and by National Aeronautics and Space Administration–Langley contract NAS1-18605.

Essentially nonoscillating (ENO) schemes have been very successful in solving the hyperbolic conservation law (1.2) (Harten and Osher [3], Harten et al. [4], Shu and Osher [7], [8]). The key idea is an adaptive stencil interpolation which automatically obtains information from the locally smoothest region, and hence yields a uniformly high-order essentially nonoscillatory approximation for piecewise smooth functions. We summarize this ENO interpolation procedure as follows.

Given point values $f(x_j)$, $j=0, \pm 1, \pm 2, \cdots$ of a (usually piecewise smooth) functions at discrete nodes x_j, we associate an rth degree polynomial $P^{f,r}_{j+1/2}(x)$ with each interval $[x_j, x_{j+1}]$, constructed inductively as follows:

(1.3) (1) $P^{f,1}_{j+1/2}(x) = f[x_j] + f[x_j, x_{j+1}](x - x_j), \qquad k_{\min} = j;$

(2) If $k^{(l-1)}_{\min}$ and $P^{f,l-1}_{j+1/2}(x)$ are both defined, then let

$$a^{(l)} = f[x_{k^{(l-1)}_{\min}}, \cdots, x_{k^{(l-1)}_{\min}+l}],$$

$$b^{(l)} = f[x_{k^{(l-1)}_{\min}-1}, \cdots, x_{k^{(l-1)}_{\min}+l-1}],$$

and

(i) If $|a^{(l)}| \geqq |b^{(l)}|$, then $c^{(l)} = b^{(l)}$, $k^{(l)}_{\min} = k^{(l-1)}_{\min} - 1$, otherwise $c^{(l)} = a^{(l)}$, $k^{(l)}_{\min} = k^{(l-1)}_{\min}$,

(ii) $$P^{f,l}_{j+1/2}(x) = P^{f,l-1}_{j+1/2}(x) + c^{(l)} \prod_{i=k^{(l-1)}_{\min}}^{k^{(l-1)}_{\min}+l-1} (x - x_i). \qquad \square$$

In the above procedure $f[\cdot, \cdots, \cdot]$ are the usual Newton divided differences. Note that we can also start from one node x_j to build a polynomial $P^{f,r}_j(x)$ using the same procedure.

In [6] Osher and Sethian constructed ENO type schemes and applied them to a class of H-J equations and perturbations, arising in front propagation problems. They achieved very good numerical results. In this paper we provide a more general ENO scheme construction procedure, mainly by considering different multidimensional monotone building blocks. We then numerically test the schemes on a variety of one- and two-dimensional problems including a problem related to control optimization, check the accuracy in smooth regions, the resolution of discontinuities in derivatives, and the phenomenon of convergence to viscosity solutions. Concluding remarks are given in § 4.

2. Scheme construction. For simplicity of exposition we take $d=2$ in (1.1), and use x, y instead of x_1, x_2:

(2.1) $$\phi_t + H(\phi_x, \phi_y) = 0, \qquad \phi(x, y, 0) = \phi_0(x, y).$$

For mesh sizes $\Delta x, \Delta y, \Delta t$, ϕ^n_{ij} will denote a numerical approximation to the viscosity solution $\phi(x_i, y_j, t^n) = \phi(i\Delta x, j\Delta y, n\Delta t)$ of (2.1). We also use standard notation such as

$$\lambda_x = \frac{\Delta t}{\Delta x}, \quad \lambda_y = \frac{\Delta t}{\Delta y}, \quad \Delta^x_{\pm}\phi_{ij} = \pm(\phi_{i\pm1,j} - \phi_{ij}), \quad \Delta^y_{\pm}\phi_{ij} = \pm(\phi_{i,j\pm1} - \phi_{ij}).$$

We start with a first-order monotone scheme [2]:

(2.2) $$\phi^{n+1}_{ij} = \phi^n_{ij} - \Delta t \hat{H}\left(\frac{\Delta^x_+\phi^n_{ij}}{\Delta x}, \frac{\Delta^x_-\phi^n_{ij}}{\Delta x}, \frac{\Delta^y_+\phi^n_{ij}}{\Delta y}, \frac{\Delta^y_-\phi^n_{ij}}{\Delta y}\right)$$

where $\hat{H}$ is a Lipschitz continuous monotone flux consistent with H:

$$\hat{H}(u, u, v, v) = H(u, v).$$

Monotonicity here means that $\hat{H}$ is nonincreasing in its first and third arguments and nondecreasing in the other two. Symbolically, $H(\downarrow, \uparrow, \downarrow, \uparrow)$.

We now give some examples of monotone fluxes $\hat{H}$:

(1) Lax-Friedrichs [2]:

$$\hat{H}^{\mathrm{LF}}(u^+, u^-, v^+, v^-) = H\left(\frac{u^+ + u^-}{2}, \frac{v^+ + v^-}{2}\right) - \frac{1}{2}\alpha^x(u^+ - u^-) - \frac{1}{2}\alpha^y(v^+ - v^-) \tag{2.3}$$

where

$$\alpha^x = \max_{\substack{A \leqq u \leqq B \\ C \leqq v \leqq D}} |H_1(u, v)|, \qquad \alpha^y = \max_{\substack{A \leqq u \leqq B \\ C \leqq v \leqq D}} |H_2(u, v)|. \tag{2.4}$$

Here $H_i(u, v)$ is the partial derivative of H with respect to the ith argument. The flux $\hat{H}^{\mathrm{LF}}$ is monotone for $A \leqq u^{\pm} \leqq B$, $C \leqq v^{\pm} D \leqq D$.

(2) Godunov type [5]:

$$\hat{H}^G(u^+, u^-, v^+, v^-) = \operatorname*{ext}_{u \in I(u^-, u^+)} \operatorname*{ext}_{v \in I(v^-, v^+)} H(u, v) \tag{2.5}$$

where

$$I(a, b) = [\min(a, b), \max(a, b)] \tag{2.6}$$

and the function ext is defined by

$$\operatorname*{ext}_{u \in I(a,b)} = \begin{cases} \min\limits_{a \leqq u \leqq b} & \text{if } a \leqq b, \\ \max\limits_{b \leqq u \leqq a} & \text{if } a > b. \end{cases} \tag{2.7}$$

As pointed out in [5], since in general $\min_u \max_v H(u, v) \neq \max_v \min_u H(u, v)$, we will generally obtain different versions of Godunov type fluxes $\hat{H}^G$, by changing the order of min and max. Uniqueness of $\hat{H}^G$ happens when, e.g., $H(u, v) = H^1(u) + H^2(v)$, and in many other cases. Then, by [5], $-t\hat{H}^G(u, v)$ is the exact solution to the Riemann problem of (2.1), i.e., this is the viscosity solution of (2.1) for

$$\phi_0(x, y) = xu_0(x) + yv_0(y),$$

$$u_0(x) = \begin{cases} u^+, & x \geqq 0, \\ u^-, & x < 0, \end{cases} \qquad v_0(y) = \begin{cases} v^+, & y \geqq 0, \\ v^-, & y < 0, \end{cases} \tag{2.8}$$

evaluated at $(x, y) = (0, 0)$, and $t > 0$.

For this reason all monotone fluxes can be regarded as approximate Riemann solvers in this sense.

(3) Local Lax-Friedrichs (LLF) [8]:

$$\begin{aligned} \hat{H}^{\mathrm{LLF}}(u^+, u^-, v^+, v^-) = H\left(\frac{u^+ + u^-}{2}, \frac{v^+ + v^-}{2}\right) - \frac{1}{2}\alpha^x(u^+, u^-)(u^+ - u^-) \\ - \frac{1}{2}\alpha^y(v^+, v^-)(v^+ - v^-) \end{aligned} \tag{2.9}$$

where

$$\alpha^x(u^+, u^-) = \max_{\substack{u \in I(u^-, u^+) \\ C \leqq v \leqq D}} |H_1(u, v)|, \qquad \alpha^y(v^+, v^-) = \max_{\substack{v \in I(v^-, v^+) \\ A \leqq u \leqq B}} |H_2(u, v)|. \tag{2.10}$$

In the Appendix we prove that $\hat{H}^{\mathrm{LLF}}$ is monotone for $A \leqq u^{\pm} \leqq B$, $C \leqq v^{\pm} \leqq D$; Note that $\hat{H}^{\mathrm{LLF}}$ has smaller dissipation than $\hat{H}^{\mathrm{LF}}$.

(4) Roe with LLF entropy correction [8]:

$$\text{(2.11)}\quad \hat{H}^{\mathrm{RF}}(u^+, u^-, v^+, v^-) = \begin{cases} H(u^*, v^*) \\ \quad \text{if } H_1(u, v) \text{ and } H_2(u, v) \text{ do not change signs in} \\ \quad\quad u \in I(u^-, u^+),\ v \in I(v^-, v^+), \\ H\left(\dfrac{u^+ + u^-}{2}, v^*\right) - \dfrac{1}{2}\alpha^x(u^+, u^-)(u^+ - u^-); \\ \quad \text{otherwise and if } H_2(u, v) \text{ does not change sign in} \\ \quad\quad A \leqq u \leqq B,\ v \in I(v^-, v^+), \\ H\left(u^*, \dfrac{v^+ + v^-}{2}\right) - \dfrac{1}{2}\alpha^y(v^+, v^-)(v^+ - v^-); \\ \quad \text{otherwise and if } H_1(u, v) \text{ does not change sign in} \\ \quad\quad u \in I(u^-, u^+),\ C \leqq v \leqq D, \\ \hat{H}^{\mathrm{LLF}}(u^+, u^-, v^+, v^-) \quad \text{otherwise} \end{cases}$$

where u^*, v^* are defined by upwinding:

$$\text{(2.12)}\qquad u^* = \begin{cases} u^+ & \text{if } H_1(u, v) \leqq 0, \\ u^- & \text{if } H_1(u, v) \geqq 0, \end{cases} \qquad v^* = \begin{cases} v^+ & \text{if } H_2(u, v) \leqq 0, \\ v^- & \text{if } H_2(u, v) \geqq 0. \end{cases}$$

We will prove in the Appendix that $\hat{H}^{\mathrm{RF}}$ is monotone for $A \leqq u^{\pm} \leqq B$, $C \leqq v^{\pm} \leqq D$. Note that $\hat{H}^{\mathrm{RF}}$ is simple to code, purely upwinding, with almost as small dissipation as $\hat{H}^G$. Also note that $\hat{H}^{\mathrm{RF}}$ is not continuous: for example if $H(u) = u^2/2$ (one space dimension) then $\hat{H}^{\mathrm{RF}}(1, 0) = 0$ but

$$\hat{H}^{\mathrm{RF}}(1, -\varepsilon) = \frac{((1-\varepsilon)/2)^2}{2} - \frac{1}{2} \cdot 1 \cdot (1+\varepsilon) \xrightarrow{\varepsilon \to 0^+} -\frac{3}{8} \neq 0.$$

However, this type of discontinuity does not hurt, because we have

$$\text{(2.13)}\quad |\hat{H}^{\mathrm{RF}}(u^+, u^-, v^+, v^-) - \hat{H}^G(u^+, u^-, v^+, v^-)| \leqq M(|u^+ - u^-| + |v^+ - v^-|);$$

hence we still get consistency and accuracy.

Remark 2.1. A flux with even smaller dissipation than $\hat{H}^{\mathrm{LLF}}$ is

$$\text{(2.14)}\quad \hat{H}^{\mathrm{LLLF}}(u^+, u^-, v^+, v^-) = H\left(\frac{u^+ + u^-}{2}, \frac{v^+ + v^-}{2}\right) - \frac{1}{2}\alpha^x(u^{\pm}, v^{\pm})(u^+ - u^-) - \frac{1}{2}\alpha^y(u^{\pm}, v^{\pm})(v^+ - v^-)$$

where

$$\text{(2.15)}\quad \alpha^x(u^{\pm}, v^{\pm}) = \max_{\substack{u \in I(u^-, u^+) \\ v \in I(v^-, v^+)}} |H_1(u, v)|, \qquad \alpha^y(u^{\pm}, v^{\pm}) = \max_{\substack{u \in I(u^-, u^+) \\ v \in I(v^-, v^+)}} |H_2(u, v)|.$$

Unfortunately it is not monotone: for example, if $H(u, v) = e^{u+v}$, then $\hat{H}^{\mathrm{LLLF}}(2, 0, 0, 20) > \hat{H}^{\mathrm{LLLF}}(0, 0, 0, 20)$. For separable Hamiltonians with $H(u, v) = H^1(u) + H^2(v)$ we have $\hat{H}^{\mathrm{LLLF}} = \hat{H}^{\mathrm{LLF}}$.

We now begin the description of our high-order ENO schemes. Monotone fluxes play the role of "building blocks." The ENO interpolation idea in (1.3) is used to obtain high-order nonoscillatory approximations to $u^{\pm} = \phi_x^{\pm}$ and $v^{\pm} = \phi_y^{\pm}$. These values are then put into a monotone flux $\hat{H}(u^+, u^-, v^+, v^-)$. Time accuracy is obtained by a

class of TVD Runge-Kutta type time discretizations [7]. We summarize the algorithm as follows.

ALGORITHM 2.1.

(1) At any node (i,j), fix j to compute along the x-direction, by using (1.3), obtaining

$$u_{ij}^{\pm} = \frac{d}{dx} P_{i\pm 1/2,j}^{\phi,r}(x_i). \tag{2.16}$$

Similarly for $v_{ij}^{\pm}$. Then let

$$L_{ij} = -\Delta t \hat{H}(u_{ij}^{+}, u_{ij}^{-}, v_{ij}^{+}, v_{ij}^{-}). \tag{2.17}$$

(2) Obtain ϕ^{n+1} from ϕ^n by the following Runge-Kutta type procedure:

$$\phi_{ij}^{(k)} = \sum_{l=0}^{k-1} [\alpha_{kl}\phi_{ij}^{(l)} + \beta_{kl} L_{ij}^{(l)}], \qquad k = 1, \cdots, \bar{r}, \tag{2.18a}$$

$$\phi_{ij}^{(0)} = \phi_{ij}^{n}, \qquad \phi_{ij}^{(\bar{r})} = \phi_{ij}^{n+1}. \tag{2.18b}$$

□

We can take $\bar{r} = r$ and positive α_{kl} and β_{kl} for up to third-order $r \leqq 3$. The method (2.18) can be proven TVD under the CFL condition

$$\lambda = \frac{\Delta t}{\Delta x} \leqq C_r \lambda_0 \tag{2.19}$$

if the Euler forward version of (2.17) is TVD under the CFL condition

$$\lambda = \frac{\Delta t}{\Delta x} \leqq \lambda_0. \tag{2.20}$$

We summarize some of the schemes (2.18) in Table 2.1.

Algorithm 2.1 is formally uniformly rth order in space and time in smooth regions (measured by local truncation errors).

Note that in the algorithm above, we need to evaluate two polynomials $P_{i\pm 1/2,j}^{\phi,r}$ to get $u^{\pm}$. If the monotone flux is purely upwind and there is no "sonic point" (a point

TABLE 2.1
TVD *Runge-Kutta method* (2.19).

Order	α_{kl}	β_{kl}	C_r
2	$\begin{matrix} 1 & \\ \frac{1}{2} & \frac{1}{2} \end{matrix}$	$\begin{matrix} 1 & \\ 0 & \frac{1}{2} \end{matrix}$	1
3	$\begin{matrix} 1 & & \\ \frac{3}{4} & \frac{1}{4} & \\ \frac{1}{3} & 0 & \frac{2}{3} \end{matrix}$	$\begin{matrix} 1 & & \\ 0 & \frac{1}{4} & \\ 0 & 0 & \frac{2}{3} \end{matrix}$	1
4	$\begin{matrix} 1 & & & \\ \frac{1}{2} & \frac{1}{2} & & \\ \frac{1}{9} & \frac{2}{9} & \frac{2}{3} & \\ 0 & \frac{1}{3} & \frac{1}{3} & \frac{1}{3} \end{matrix}$	$\begin{matrix} \frac{1}{2} & & & \\ -\frac{1}{4} & \frac{1}{2} & & \\ -\frac{1}{9} & -\frac{1}{3} & 1 & \\ 0 & \frac{1}{6} & 0 & \frac{1}{6} \end{matrix}$	$\frac{2}{3}$

at which H_1 or H_2 changes sign), one of u^+ and u^- is never used. We thus recommend the following algorithm.

ALGORITHM 2.2.

(1) Compute $\tilde{u}_{ij}^{\pm} = \Delta_{\pm}^x \phi_{ij}^n / \Delta x$ and $\tilde{v}_{ij}^{\pm} = \Delta_{\pm}^y \phi_{ij}^n / \Delta y$. If $H_1(u, v)$ and $H_2(u, v)$ do not change signs in $u \in I(\tilde{u}_{ij}^-, \tilde{u}_{ij}^+)$, $v \in I(\tilde{v}_{ij}^-, \tilde{v}_{ij}^+)$, then compute only u_{ij}^* and v_{ij}^* by (2.16) where u^*, v^* are defined by (2.12); and take $L_{ij} = -\Delta t H(u^*, v^*)$; otherwise take (2.17).

(2) Same as step (2) in Algorithm 2.1. □

Note that Algorithm 2.2 is NOT equivalent to Algorithm 2.1 with $\hat{H} = \hat{H}^{\mathrm{RF}}$. Since we expect sonic points to be isolated, Algorithm 2.2 is usually almost twice as fast as Algorithm 2.1.

Remark 2.2. Note that, in smooth regions, by Taylor expansion,

$$\frac{d}{dx} P_{i\pm 1/2}^{\phi, r}(x_i) - \frac{\Delta_{\pm}\phi_i}{\Delta x} = \frac{\Delta x}{2} \phi_{xx}(\xi). \tag{2.21}$$

If we choose, instead of (2.16),

$$u_{ij}^{\pm} = \mathbb{P}_{[\Delta_{\pm}^x \phi_{ij}/\Delta x, M\Delta x]}\left(\frac{d}{dx} P_{i\pm\frac{1}{2},j}^{\phi, r}(x_i)\right) \tag{2.22}$$

where the projection $\mathbb{P}$ is defined by

$$\mathbb{P}_{[a,b]}(y) = \begin{cases} y & \text{if } a - b \leqq y \leqq a + b, \\ a - b & \text{if } y < a - b, \\ a + b & \text{if } y > a + b, \end{cases} \tag{2.23}$$

we will still have uniform high-order accuracy $u_{ij}^{\pm} = (\phi_x)_{ij} + O(\Delta x^r)$ in any region where $|\phi_{xx}| \leqq 2M$. Algorithm 2.1 will then give a scheme which deviates from a monotone scheme by $M\Delta t \Delta x$; hence we trivially obtain convergence to the viscosity solution through the theory for monotone schemes. In practice we do not recommend (2.22), because the parameter M is not intrinsic—it has to be adjusted for each individual problem. See [7, p. 452] for a discussion of a similar situation for conservation laws.

Remark 2.3. When implementing (1.3) we use undivided differences:

$$\varphi(j, 0) = \varphi_j, \tag{2.24a}$$

$$\varphi(j, k) = \varphi(j+1, k-1) - \varphi(j, k-1), \qquad k = 1, \cdots, r+1. \tag{2.24b}$$

The computation of (2.24) can be easily vectorized. The ENO stencil-choosing process is, for computing $u^+ = (\varphi_x)^+$, starting with $i(j) = j$ and performing

$$\text{if (abs } (\varphi(i(j), k)). \text{ gt. abs } (\varphi(i(j)-1, k))), \qquad i(j) = i(j) - 1 \tag{2.25}$$

for $k = 2, \cdots, r$, where $i(j)$ is the leftmost point in the stencil for $P_{j+1/2}^{\varphi, r}(x)$. This can also be vectorized. Finally,

$$u_j^+ = (\varphi_x)_j^+ = \frac{1}{\Delta x} \sum_{k=1}^{r} c(i(j) - j, k) \varphi(i(j), k) \tag{2.26}$$

where

$$c(m, k) = \frac{1}{k!} \sum_{s=m}^{m+k-1} \prod_{\substack{l=m \\ l \neq s}}^{m+k-1} (-l). \tag{2.27}$$

Note that the small matrix c is independent of φ, is only computed once, and then is stored. Equation (2.26) can be vectorized easily as well.

3. Numerical results.

Example 1 (One dimension). We solve

$$\begin{aligned} &\phi_t + H(\phi_x) = 0, \\ &\phi(x, 0) = -\cos \pi x, \end{aligned} \qquad -1 \leqq x < 1 \tag{3.1}$$

with a convex H (Burgers' equation):

$$H(u) = \frac{(u+\alpha)^2}{2} \tag{3.2}$$

and a nonconvex H:

$$H(u) = -\cos(u+\alpha). \tag{3.3}$$

Note that if we let $v = \phi_x + \alpha$, $f(v) = H(v-\alpha)$, then (3.1) becomes a conservation law

$$\begin{aligned} &v_t + f(v)_x = 0, \\ &v(x, 0) = \alpha + \pi \sin \pi x, \end{aligned} \qquad -1 \leqq x < 1, \tag{3.4}$$

which is a standard test problem for conservation laws (e.g., [7]). We can easily use the method of characteristics to obtain the exact solution of (3.1) through that of (3.4).

We take $\alpha = 1$ and compute the result to $t = t_1 = 0.5/\pi^2$ (when the solution is still smooth) and to $t = t_2 = 1.5/\pi^2$ (when the solution has a discontinuous derivative). We print out the L_1 and L_∞ errors, in Table 3.1, for selected first-order monotone schemes and third-order ENO schemes in smooth regions, i.e., the whole region $[-1, 1]$ for $t = t_1$ and the region $|x - x_s| \geqq 0.1$ for $t = t_2$ where x_s is the location of any discontinuity of the derivative. We also present the graphs of the numerical solutions (in diamonds) versus the exact solutions (in solid lines) in Figs. 1 and 2.

Remark 3.1. From Table 3.1 and Figs. 1 and 2 we can observe the following:

(i) The resolution of third-order ENO schemes with 10 points is roughly the same as that of the corresponding monotone schemes with 80 points;

(ii) ENO-3-Godunov and ENO-3-RF have roughly the same resolution, even if the latter is much simpler than the former and only takes about half time.

Example 2 (Two dimensions). We solve

$$\begin{aligned} &\phi_t + H(\phi_x, \phi_y) = 0, \\ &\phi(x, y, 0) = -\cos \pi\left(\frac{x+y}{2}\right), \end{aligned} \qquad -2 \leqq x, y \leqq 2 \tag{3.5}$$

with a convex H (Burgers' equation):

$$H(u, v) = \frac{(u+v+\alpha)^2}{2} \tag{3.6}$$

and a nonconvex H:

$$H(u, v) = -\cos(u+v+\alpha). \tag{3.7}$$

Note that, under the transformation $\xi = (x+y)/2$, $\eta = (x-y)/2$, (3.5)-(3.7) become (3.1)-(3.3) in the ξ direction. We can thus use the one-dimensional exact solution to analyze our numerical results. Since we use (x, y) coordinates, this is a true two-dimensional test problem.

We again take $\alpha = 1$ and compute to $t = t_1 = 0.5/\pi^2$ and $t = t_2 = 1.5/\pi^2$. Some results are presented in Table 3.2 and Fig. 3.

TABLE 3.1
L_1 and L_∞ errors in smooth regions for (3.1).

Time			$t = 0.5/\pi^2$				$t = 1.5/\pi^2$			
	No. of points		10	20	40	80	10	20	40	80
Burger's equation $H(u) = (u+1)^2/2$	LF	L_1	1.01 (−1)	5.10 (−2)	2.59 (−2)	1.31 (−2)	2.01 (−1)	1.13 (−1)	6.11 (−2)	3.16 (−2)
		L_∞	1.81 (−1)	1.08 (−1)	6.03 (−2)	3.23 (−2)	3.17 (1−1)	1.72 (−1)	8.48 (−2)	4.58 (−2)
	Godunov	L_1	3.36 (−2)	1.50 (−2)	7.66 (−3)	3.87 (−3)	5.94 (−2)	3.18 (−2)	1.70 (−2)	8.50 (−3)
		L_∞	7.40 (−2)	3.61 (−2)	1.93 (−2)	1.01 (−2)	1.12 (−1)	5.93 (−2)	3.00 (−2)	1.51 (−2)
	ENO-3-LF	L_1	1.13 (−2)	1.83 (−3)	2.59 (−4)	4.27 (−5)	1.65 (−2)	2.32 (−3)	2.61 (−4)	4.17 (−5)
		L_∞	3.16 (−2)	5.08 (−3)	8.75 (−4)	2.07 (−4)	3.40 (−2)	7.81 (−3)	1.33 (−3)	1.07 (−4)
	ENO-3-God	L_1	5.74 (−3)	9.55 (−4)	1.41 (−4)	2.56 (−5)	7.37 (−3)	1.18 (−3)	1.46 (−4)	2.85 (−5)
		L_∞	1.52 (−2)	4.48 (−3)	7.55 (−4)	1.52 (−4)	2.29 (−2)	6.76 (−3)	9.79 (−4)	1.04 (−4)
	ENO-3-RF	L_1	5.79 (−3)	9.56 (−4)	1.42 (−4)	2.56 (−5)	8.19 (−3)	1.15 (−3)	1.46 (−4)	2.85 (−5)
		L_∞	1.52 (−2)	4.48 (−3)	7.55 (−4)	1.52 (−4)	2.29 (−2)	5.92 (−3)	9.97 (−4)	1.04 (−4)
Nonconvex $H(u) = -\cos(u+1)$	LF	L_1	2.70 (−2)	1.19 (−2)	5.56 (−3)	2.58 (−3)	5.51 (−2)	2.83 (−2)	1.33 (−2)	6.43 (−3)
		L_∞	4.15 (−2)	2.36 (−2)	1.30 (−2)	6.98 (−3)	1.03 (−1)	4.72 (−2)	2.29 (−2)	1.12 (−2)
	Godunov	L_1	1.52 (−2)	5.89 (−3)	2.46 (−3)	1.16 (−3)	2.41 (−2)	1.13 (−2)	5.45 (−3)	2.60 (−3)
		L_∞	3.52 (−2)	1.22 (−2)	5.88 (−3)	2.57 (−3)	4.69 (−2)	2.56 (−2)	1.26 (−2)	5.78 (−3)
	ENO-3-LF	L_1	1.62 (−3)	5.68 (−4)	8.92 (−5)	9.47 (−6)	8.81 (−3)	1.35 (−3)	1.84 (−4)	2.43 (−5)
		L_∞	6.23 (−3)	2.33 (−3)	4.81 (−4)	1.06 (−4)	1.39 (−2)	9.07 (−3)	1.53 (−3)	2.14 (−4)
	ENO-3-God	L_1	1.05 (−3)	3.17 (−4)	5.92 (−5)	7.57 (−6)	7.05 (−3)	9.10 (−4)	1.51 (−4)	2.56 (−5)
		L_∞	3.13 (−3)	1.17 (−3)	2.66 (−4)	4.39 (−5)	1.31 (−2)	5.93 (−3)	1.39 (−3)	2.01 (−4)
	ENO-3-RF	L_1	1.11 (−3)	3.21 (−4)	5.92 (−5)	7.57 (−6)	6.31 (−3)	9.10 (−4)	1.51 (−4)	2.60 (−5)
		L_∞	3.44 (−3)	1.17 (−3)	2.66 (−4)	4.39 (−5)	1.27 (−2)	5.94 (−3)	1.39 (−3)	2.01 (−4)

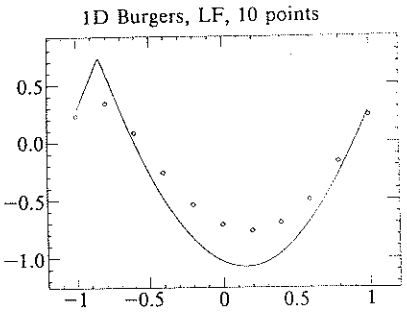

(a) *First-order Lax–Friedrichs, 10 points.*

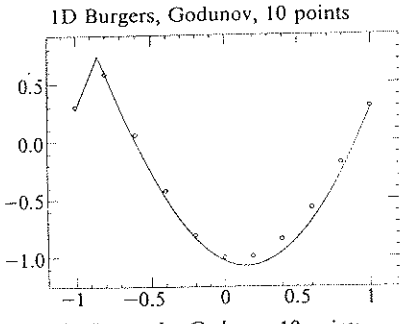

(b) *First-order Godunov, 10 points.*

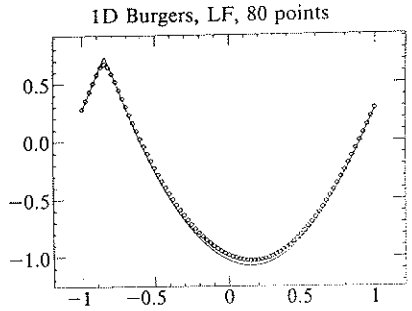

(c) *First-order Lax–Friedrichs, 80 points.*

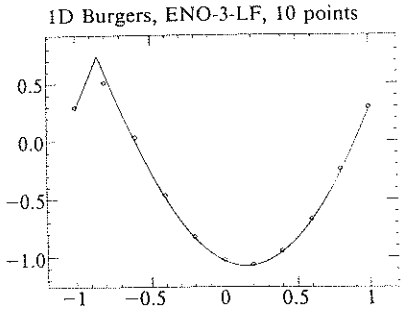

(d) *Third-order* ENO-LF, 10 *points.*

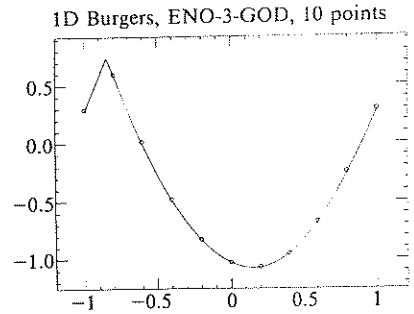

(e) *Third-order* ENO-*Godunov*, 10 *points.*

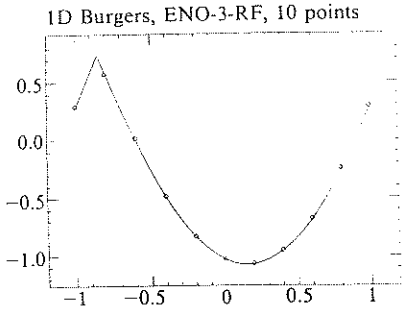

(f) *Third-order* ENO-RF, 10 *points.*

FIG. 1. *One-dimensional Burgers' equation.*

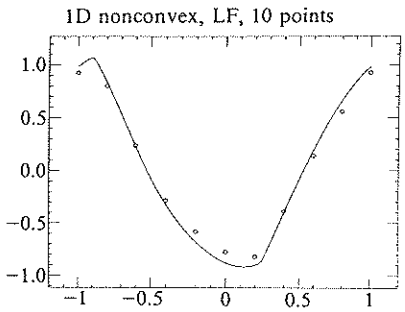

(a) *First-order Lax–Friedrichs, 10 points.*

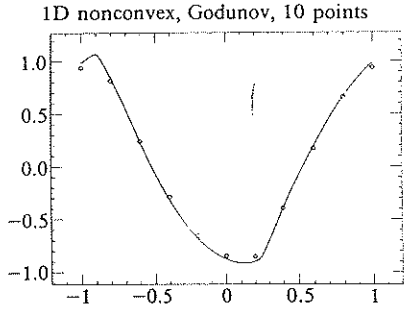

(b) *First-order Godunov, 10 points.*

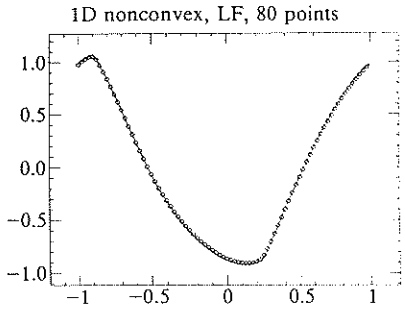

(c) *First-order, Lax–Friedrichs, 80 points.*

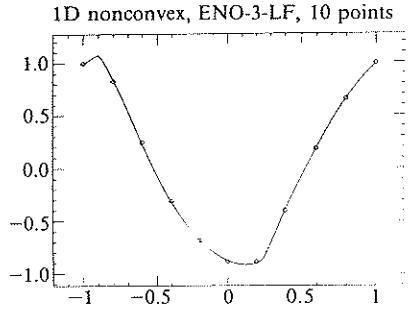

(d) *Third-order* ENO-LF, 10 *points.*

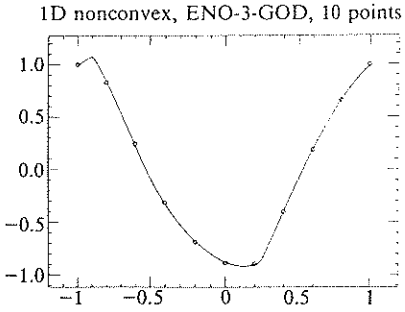

(e) *Third-order* ENO-*Godunov*, 10 *points.*

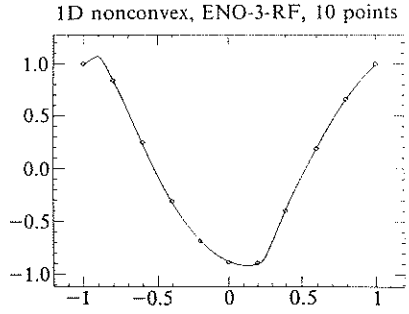

(f) *Third-order* ENO-RF, 10 *points.*

FIG. 2. *One dimension,* $H(u) = -\cos(u+1)$.

TABLE 3.2
L_1 and L_∞ errors in smooth regions for (3.5).

	Time		$t = 0.5/\pi^2$				$t = 1.5/\pi^2$			
	No. of points		10^2	20^2	40^2	80^2	10^2	20^2	40^2	80^2
$H = (u+v+1)^2/2$	LF	L_1	1.01 (−1)	5.10 (−2)	2.59 (−2)	1.31 (−2)	2.24 (−1)	1.25 (−1)	6.79 (−2)	3.51 (−2)
		L_∞	1.81 (−1)	1.08 (−1)	6.03 (−2)	3.23 (−2)	3.17 (−1)	1.72 (−1)	8.98 (−2)	4.59 (−2)
	ENO-3-LF	L_1	1.15 (−2)	1.83 (−3)	2.59 (−4)	4.25 (−5)	1.83 (−2)	2.58 (−3)	2.90 (−4)	4.64 (−5)
		L_∞	3.37 (−2)	5.09 (−3)	8.75 (−4)	2.11 (−4)	3.41 (−2)	7.82 (−3)	1.34 (−3)	1.15 (−4)
$H = \cos(u+v+1)$	LF	L_1	2.70 (−2)	1.19 (−2)	5.56 (−3)	2.58 (−3)	8.01 (−2)	3.56 (−2)	1.67 (−2)	8.03 (−3)
		L_∞	4.15 (−2)	2.36 (−2)	1.30 (−2)	6.98 (−3)	1.03 (−1)	4.72 (−2)	2.29 (−2)	1.12 (−2)
	ENO-3-LF	L_1	1.65 (−3)	5.68 (−4)	8.93 (−5)	9.23 (−6)	1.03 (−2)	1.69 (−3)	2.20 (−4)	4.93 (−5)
		L_∞	6.23 (−3)	2.33 (−3)	4.82 (−4)	1.07 (−4)	1.42 (−2)	9.10 (−3)	1.56 (−3)	6.13 (−4)

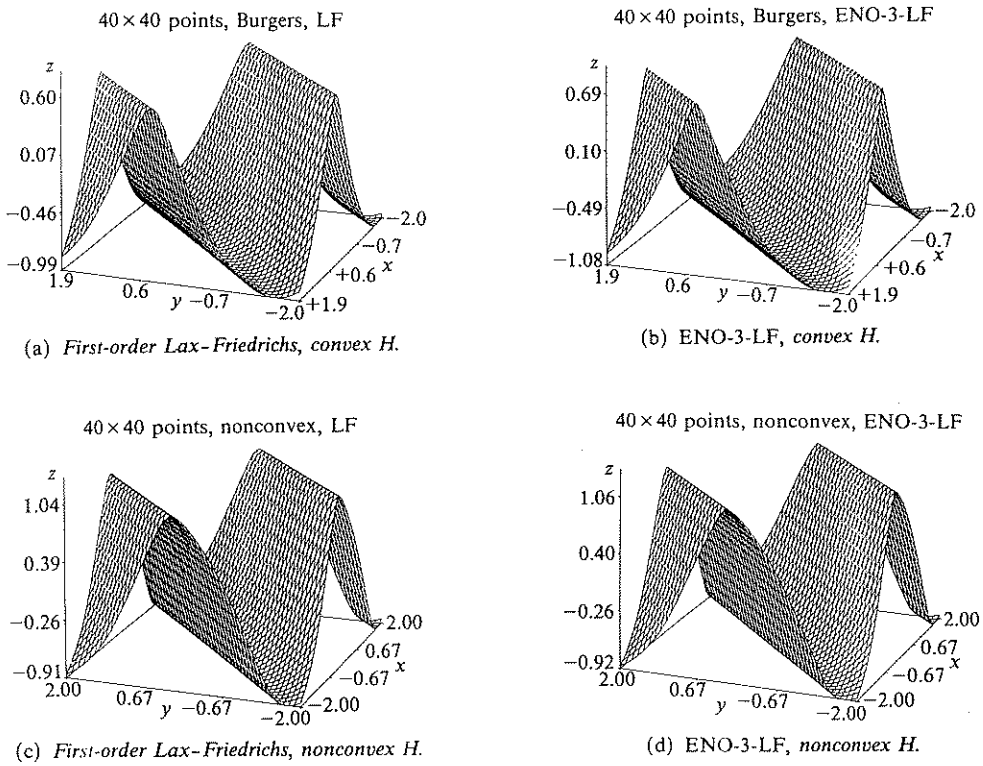

(a) *First-order Lax-Friedrichs, convex H.*

(b) ENO-3-LF, *convex H.*

(c) *First-order Lax-Friedrichs, nonconvex H.*

(d) ENO-3-LF, *nonconvex H.*

FIG. 3. *Two dimensions,* 40×40 *points.*

Remark 3.2. (i) By comparing Table 3.2 with Table 3.1 we can see that ENO schemes perform equally well in two dimensions.

(ii) Note that, except for a sharper discontinuity-in-derivative resolution, we cannot see much difference between Figs. 3(a), 3(c) (first-order monotone schemes) and 3(b), 3(d) (third-order ENO schemes). However, from Table 3.2 we can clearly see a large difference in the resolution of the solution in smooth regions. This indicates the limitations of graphical presentations.

(iii) In this two-dimensional case, the Godunov flux is considerably more complicated to program than LF or RF, with a not-so-significant improvement in resolution for ENO-3.

Example 3. We solve a two-dimensional nonconvex Riemann problem

$$\phi_t + \sin(\phi_x + \phi_y) = 0, \qquad \phi(x, y, 0) = \pi(|y| - |x|) \tag{3.8}$$

to investigate the resolutions of different building blocks, the behavior of different versions of Godunov flux (2.5); and convergence to viscosity solutions. The results are in Figs. 4 and 5. From the graphs and computer outputs we can observe the following:

(i) ENO-3 with G1, G2 (two versions of Godunov fluxes), LF and RF as building blocks are all convergent to the viscosity solution, with a much sharper resolution for the discontinuities-in-derivative than the corresponding first-order monotone schemes;

(ii) ENO-3-RF has roughly the same resolution as ENO-3-Godunov, with a much simpler program and a reduced computer cost;

(iii) The difference between two versions of Godunov fluxes is very small: the average difference at $t = 1$ is around 1,000 times smaller than the L_1 errors.

40×40 points, $t = 1.0$, LF, CB

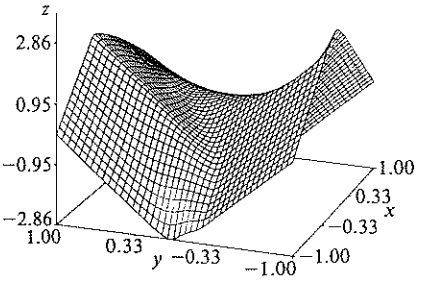

(a) *First-order Lax–Friedrichs.*

40×40 points, $t = 1.0$, ENO-3, CB

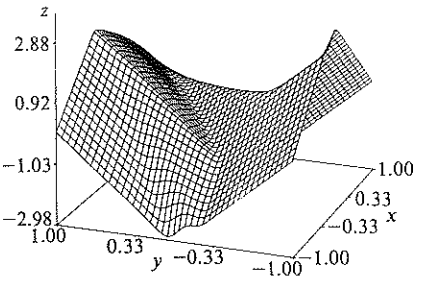

(b) ENO-3-LF.

40×40 points, $t = 1.0$, G1, CB

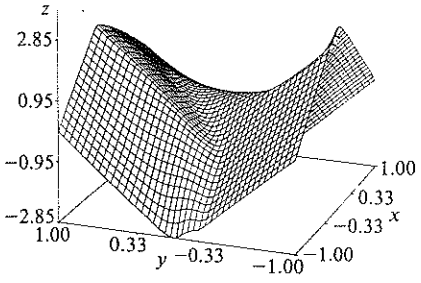

(c) *First-order, Godunov, version* I.

40×40 points, $t = 1.0$, ENO-G1-3, CB

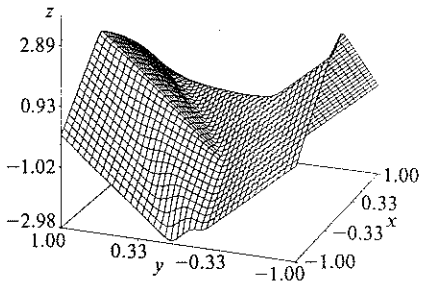

(d) ENO-3-G1.

40×40 points, $t = 1.0$, G2, CB

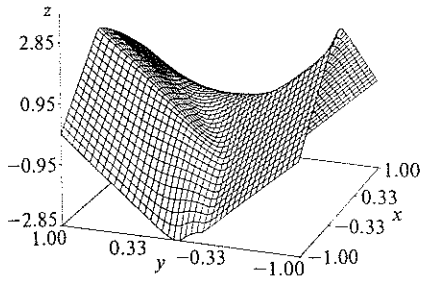

(e) *First-order Godunov, version* II.

40×40 points, $t = 1.0$, ENO-G2-3, CB

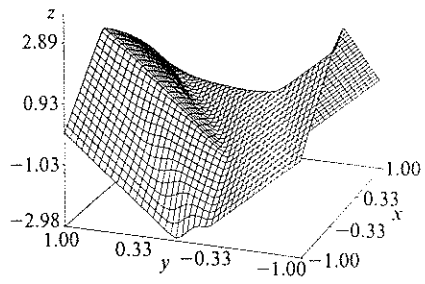

(f) ENO-3-G2.

40×40 points, $t = 1.0$, ROE-C, CB

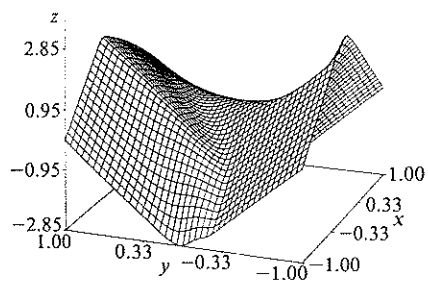

(g) *First-order Roe with entropy correction.*

40×40 points, $t = 1.0$, ENO-ROE-C-3, CB

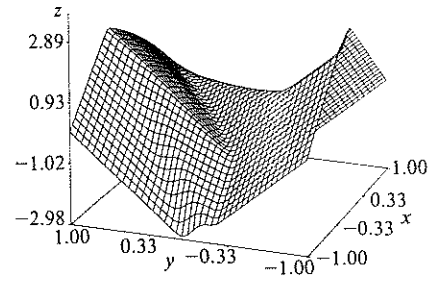

(h) ENO-3-RF.

FIG. 4. *Riemann problem* (3.8), 40×40 *points*, $t = 1$.

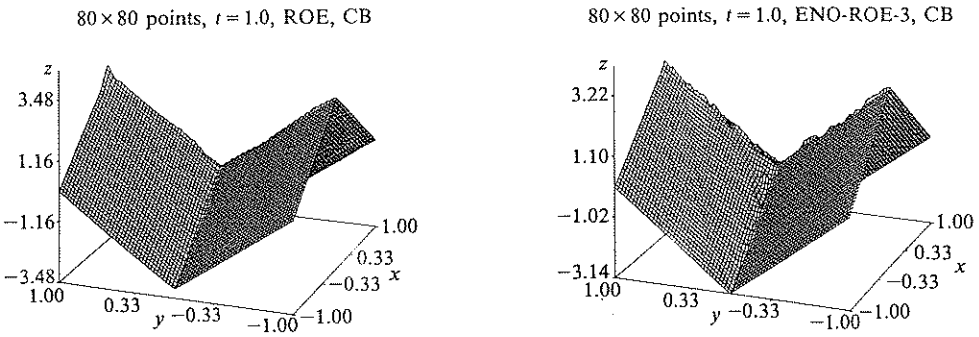

(a) *First-order Roe.* (b) ENO-3-*Roe.*

FIG. 5. *Riemann problem* (3.8), 80 × 80 *points*, $t = 1$.

(iv) ENO-3, using the Roe flux as a building block without entropy corrections, i.e., Algorithm 2.2 without using (2.17) for entropy corrections in "sonic cells," converges to an incorrect solution just as the first-order Roe scheme (Fig. 5). This indicates the importance of entropy corrections in "sonic cells."

Example 4. We solve the following problem related to control optimal cost determination:

$$\begin{aligned} &\phi_t - (\sin y)\phi_x + (\sin x + \operatorname{sign}(\phi_y))\phi_y - \tfrac{1}{2}\sin^2 y - (1-\cos x) = 0, \\ &\phi(x, y, 0) = 0, \end{aligned} \tag{3.9}$$

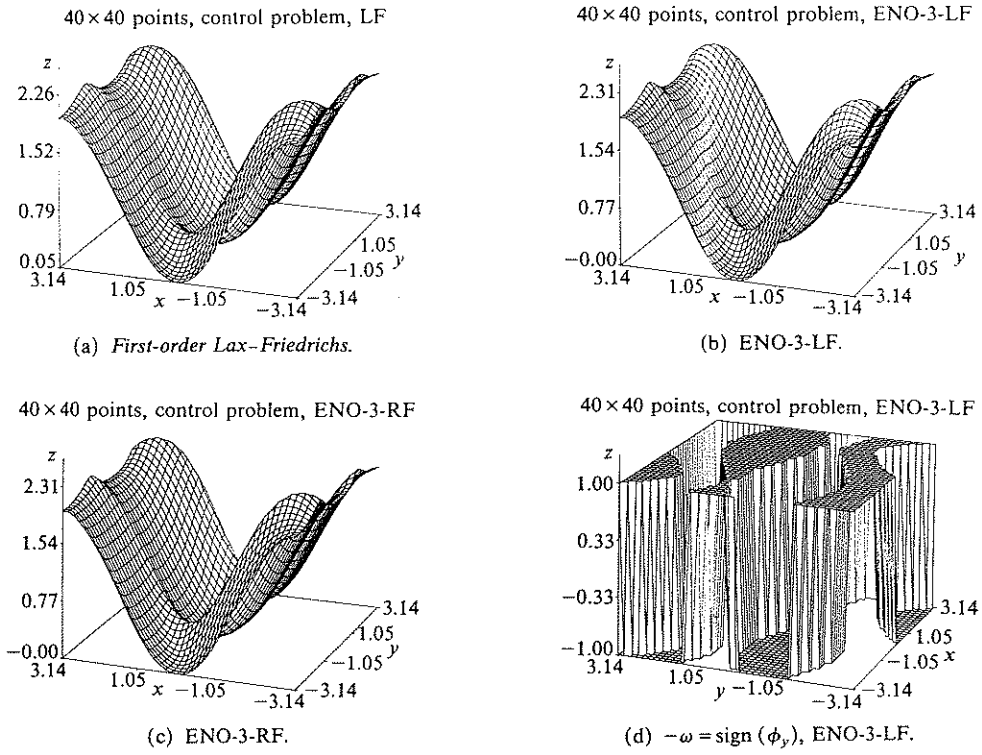

(a) *First-order Lax–Friedrichs.* (b) ENO-3-LF.

(c) ENO-3-RF. (d) $-\omega = \operatorname{sign}(\phi_y)$, ENO-3-LF.

FIG. 6. *Control problem* (3.9), 40 × 40 *points.*

assuming periodicity. The results at $t=1$ are presented in Fig. 6. Note that third-order ENO schemes have sharper discontinuities-in-derivative resolution than first-order monotone schemes. For this problem the interesting quantity is the optimal solution $w=\text{sign}(\phi_y)$, Fig. 6d). A sharper discontinuities-in-derivative resolution means smaller error for w in the neighborhood of each such point.

4. Concluding remarks. We have generalized ENO schemes for conservation laws to Hamilton–Jacobi type equations. Computational results indicate good accuracy in regions of smoothness, sharp discontinuities in derivatives, and convergence to the correct viscosity solutions. Algorithm 2.2 (ENO-RF) is usually preferred, due to its simplicity to program, reduced computational cost, and its excellent resolution, which is comparable to the results using the much more complicated Godunov type building blocks.

Appendix. We prove that $\hat{H}^{\text{LLF}}$ and $\hat{H}^{\text{RF}}$ are both monotone. To simplify the exposition we only consider the one-dimensional case. The proof for the multi-dimensional case is similar.

LEMMA A.1. *$\hat{H}^{\text{LLF}}$ is monotone.*

Proof. $\hat{H}^{\text{LLF}}$ in one dimension is defined by

$$\hat{H}^{\text{LLF}}(u^+,u^-)=H\left(\frac{u^++u^-}{2}\right)-\frac{1}{2}\max_{u\in I(u^-,u^+)}|H'(u)|(u^+-u^-). \tag{A1}$$

We assume $u_1^+>u_2^+$ and want to prove $\hat{H}^{\text{LLF}}(u_1^+,u^-)\leqq\hat{H}^{\text{LLF}}(u_2^+,u^-)$. Let $D=\hat{H}^{\text{LLF}}(u_1^+,u^-)-\hat{H}^{\text{LLF}}(u_2^+,u^-)$. This equals

$$H\left(\frac{u_1^++u^-}{2}\right)-H\left(\frac{u_2^++u^-}{2}\right)-\frac{1}{2}\max_{u\in I(u^-,u_1^+)}|H'(u)|(u_1^+-u^-)$$

$$+\frac{1}{2}\max_{u\in I(u^-,u_2^+)}|H'(u)|(u_2^+-u^-).$$

Case i. $u_1^+>u_2^+\geqq u^-$. We have, for $u^-\leqq(u_2^++u^-)/2\leqq\xi\leqq(u_1^++u^-)/2\leqq u_1^+$,

$$D=\frac{1}{2}\left[H'(\xi)(u_1^+-u_2^+)-\max_{u^-\leqq u\leqq u_1^+}|H'(u)|(u_1^+-u^-)+\max_{u^-\leqq u\leqq u_2^+}|H'(u)|(u_2^+-u^-)\right]$$

$$\leqq\frac{1}{2}\left[H'(\xi)(u_1^+-u_2^+)-\max_{u^-\leqq u\leqq u_1^+}|H'(u)|(u_1^+-u^-)+\max_{u^-\leqq u\leqq u_1^+}|H'(u)|(u_2^+-u^-)\right]$$

$$=\frac{1}{2}(u_1^+-u_2^+)\left[H'(\xi)-\max_{u^-\leqq u\leqq u_1^+}|H'(u)|\right]\leqq 0;$$

Case ii. $u^-\geqq u_1^+>u_2^+$, similar to case i;

(a) $u^-\geqq u_1^-\geqq u_2^-$, and, for $u_2^-\leqq\xi\leqq u^+$ we have

$$D=\frac{1}{2}\left[H'(\xi)(2u_1^--u_2^--u^+)+\max_{u_2^-\leqq u\leqq u^+}|H'(u)|(u^+-u_2^-)\right]$$

$$=\frac{1}{2}(u^+-u_1^-)\left[\max_{u_2^-\leqq u\leqq u^+}|H'(u)|-H'(\xi)\right]$$

$$+\frac{1}{2}(u_1^--u_2^-)\left[\max_{u_2^-\leqq u\leqq u^+}|H'(u)|+H'(\xi)\right]\geqq 0$$

or

(b) $u_1^- \geqq u^+ \geqq u_2^-$, and, since $H(u_1^-) \geqq H(u^+)$ due to the fact that $H'(u) \geqq 0$ in $[u^+, u_1^-]$, we have, for $u^+ \geqq \xi \geqq (u^+ + u_2^-)/2 \geqq u_2^-$,

$$D = H(u_1^-) - \hat{H}^{\mathrm{LLF}}(u^+, u_2^-) \geqq H(u^+) - \hat{H}^{\mathrm{LLF}}(u^+, u^-)$$

$$= \frac{1}{2}\left[H'(\xi)(u^+ - u_2^-) + \max_{u_2^- \leqq u \leqq u_2^+} |H'(u)|(u^+ - u_2^-) \right]$$

$$= \frac{1}{2}(u^+ - u_2^-)\left(\max_{u_2^- \leqq u \leqq u^+} |H'(u)| + H'(\xi) \right) \geqq 0.$$

Case iii. $\hat{H}^{\mathrm{RF}}(u^+, u_1^-) = H(u^+)$, $\hat{H}^{\mathrm{RF}}(u^+, u_2^-) = \hat{H}^{\mathrm{LLF}}(u^+, u_2^-)$. As in case (ii) we can again deduce $u^+ \geqq u_2^-$; hence, for $u_2^- \leqq (u^+ + u_2^-)/2 \leqq \xi \leqq u^+$, we have

$$D = H(u^+) - \hat{H}^{\mathrm{LLF}}(u^+, u_2^-)$$

$$= \frac{1}{2}\left[H'(\xi)(u^+ - u_2^-) - \max_{u_2^- \leqq u \leqq u^+} |H'(u)|(u^+ - u_2^-) \right] \geqq 0;$$

Case iv. $\hat{H}^{\mathrm{RF}}(u^+, u_1^-) = \hat{H}^{\mathrm{LLF}}(u^+, u_1^-)$, $\hat{H}^{\mathrm{RF}}(u^+, u_2^-) = H(u_2^-)$, similar to case (ii); *Case* v. $\hat{H}^{\mathrm{RF}}(u^+, u^-) = \hat{H}^{\mathrm{LLF}}(u^+, u_1^-)$, $\hat{H}^{\mathrm{RF}}(u^+, u_2^-) = H(u^+)$, similar to case (iii). We have proved $\hat{H}(\cdot, \uparrow)$, and similarly for $\hat{H}(\downarrow, \cdot)$. □

Acknowledgment. We thank Professor Kazufumi Ito for suggesting Example 4 in § 3, and for many helpful discussions.

REFERENCES

[1] M. CRANDALL AND P. LIONS, *Viscosity solutions of Hamilton-Jacobi equations*, Trans. Amer. Math. Soc., 277 (1983), pp. 1–42.

[2] ———, *Two approximations of solutions of Hamilton-Jacobi equations*, Math. Comput., 43 (1984), pp. 1–19.

[3] A. HARTEN AND S. OSHER, *Uniformly high order accurate non-oscillatory schemes*, I, SIAM J. Numer. Anal., 24 (1987), pp. 279–309.

[4] A. HARTEN, B. ENGQUIST, S. OSHER, AND S. CHAKRAVARTHY, *Uniformly high order accurate essentially non-oscillatory schemes*, III, J. Comput. Phys., 71 (1987), pp. 231–303.

[5] S. OSHER, *The nonconvex multi-dimensional Riemann problem for Hamilton-Jacobi equations*, ICASE Report 89-53, ICASE-NASA Langley Research Center, Hampton, VA, 1989.

[6] S. OSHER AND J. SETHIAN, *Fronts propagating with curvature dependent speed: algorithms based on Hamilton-Jacobi formulations*, J. Comput. Phys., 79 (1988), pp. 12–49.

[7] C.-W. SHU AND S. OSHER, *Efficient implementation of essentially non-oscillatory shock-capturing schemes*, J. Comput. Phys., 77 (1988), pp. 439–471.

[8] ———, *Efficient implementation of essentially non-oscillatory shock-capturing schemes*, II, J. Comput. Phys., 83 (1989), pp. 32–78.